

Solar radiometry

CLAUS FRÖHLICH¹

Abstract

The classical radiometry for total solar irradiance (TSI) measurements is described using examples of the four types of radiometers currently used in space. The design, characterization and operation of these radiometers are described. Besides the instrumental characteristics determining the measurement uncertainties, an important issue is possible long-term changes of the radiometers exposed to solar irradiance—especially in the EUV—and the space environment. A model for the degradation has been developed which can explain the behaviour of most radiometers in space. The TSI record since 1978 from different platforms and radiometers can be combined in a composite time series which demonstrates that although the assumed uncertainty of the present state-of-the-art radiometers is insufficient, their short- and long-term precision is good enough to produce a reliable time series of TSI over almost 30 years.

Introduction

The term solar radiometry is generally used to refer to measurements of the “solar constant”, the total solar irradiance (TSI), integrated over all wavelengths and reduced to the mean Sun-Earth distance, 1 ua; it is an observation of the Sun as a star. The Smithsonian Astrophysical Observatory initiated a ground-based programme for the determination of solar irradiance variability already in 1902, but they were not able to distinguish between solar and atmospheric effects (see, e.g., [Abbot 1952](#); [Aldrich and Hoover 1954](#)). It was not so much a problem of solar radiometry—accurate pyrhelimeters have been known since the late 19th century (e.g., [Fröhlich 1991](#))—but of the atmospheric extinction. Measurements from high-flying aircrafts and balloons and from outside the atmosphere, i.e., from rockets and satellites, started in the sixties and yielded first results about the inconstant solar constant, see, e.g., [Drummond et al \(1968\)](#); [Plamondon \(1969\)](#); [Willson \(1972\)](#) and for a review [Fröhlich \(1977\)](#). However, a reliable record of TSI started only in November 1978, when *NIMBUS7* was launched with an electrically calibrated

¹Physikalisch-Meteorologisches Observatorium Davos, World Radiation Center, Davos Dorf, Switzerland

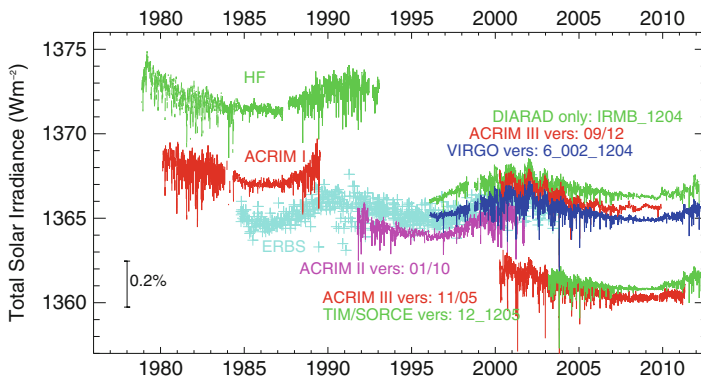


Figure 32.1: Measurements of TSI since November 1978 are plotted as originally published. During the solar activity minimum in 1986 the three data sets ranged from (1364. . . 1371) W m^{-2} , whereas during the next minimum in 1996 the range was already reduced to about 2 W m^{-2} . At that time, the measurements were within their stated relative uncertainties of the order of $\pm 0.1\%$ to $\pm 0.2\%$ and it was generally agreed that the characterization of the ECRs had improved, especially the determination of the aperture area. With the advent of the results from TIM on *SORCE* the community has been faced with a serious problem: TIM is measuring almost 5 W m^{-2} lower. The reason is due to the arrangement of the apertures and scattered light by the view-limiting aperture in the classic radiometer. The new version of ACRIM III (Version 11/05) confirms this as it includes LASP/TRF determined scattering, diffraction and basic scale calibration adjustments (for details see page 572).

radiometer (ECR) on board. All the measurements from the radiometers in space since then are shown in Figure 32.1, which illustrates the evolution of the state-of-the-art and the improvement in understanding this aspect of solar radiometry.

In the following we will describe the classical radiometry for TSI measurements using examples of the four types of radiometers currently used in space. Besides the instrumental characteristics determining the uncertainties, an important issue is possible long-term changes of the radiometers exposed to solar irradiance in the space environment. A short discussion of the resulting composites— attempts to combine all the existing time series into a contiguous one— will conclude “Solar radiometry”.

Principles and characterization of solar radiometers

Solar radiometers are based on the conversion of radiation to thermal energy which is measured by an electrically calibrated thermal flux meter. Cavities are used to improve the absorption of solar radiation. They have an aperture, called a “precision” aperture, which determines the flux-defining area, and a shutter, which opens and closes alternately while the thermal flux to the heat sink is maintained constant; this is called the active mode of operation, hence the name active cavity

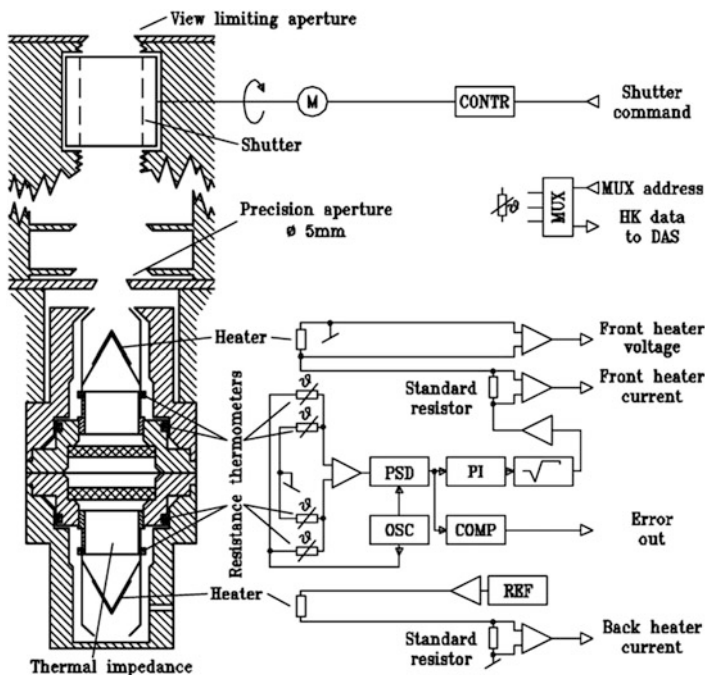


Figure 32.2: Schematic diagram of the PMO6V radiometer with its control electronics. The shutter behind the view limiting aperture is a drum which can be closed by turning it by 90° . The electronics control the active mode operation in which the heat flux (temperature difference across the thermal impedance of the front cavity) is maintained constant during the illuminated and reference phases.

radiometer (ACR). Four types are currently used in space: ACRIM-III on *ACRIM-Sat* (Willson 1979, 2001), PMO6V and DIARAD within VIRGO on *SOHO* (Brusa and Fröhlich 1986; Crommelynck et al 1987; Fröhlich et al 1995, 1997) and TIM on *SORCE* (Kopp and Lawrence 2005; Kopp et al 2005b). These references may be consulted for details of the construction of the radiometers, of their characterization and on how the uncertainties are determined. Before we discuss the differences and similarities of the different approaches, we introduce the principle of solar radiometers with the PMO6V radiometer as an example. Figure 32.2 from Fröhlich et al (1995) shows a cut through the radiometer and a block diagram of the control and measurement electronics. The front cavity is used to measure the radiation and the rear facing one is the compensating part of the differential heat flux meter; in this configuration the back cavity cannot be used for radiation measurements. In contrast DIARAD and TIM have all cavities side by side which allows radiation measurements with any of them alternatively. The active mode operation with a shutter open-closed cycle of 60 s/60 s is realized with the control circuit consisting of a Wheatstone bridge with the four wire-wound thermometers, a phase-sensitive detector (PSD) for the error signal, a proportional-integral (PI) control and a

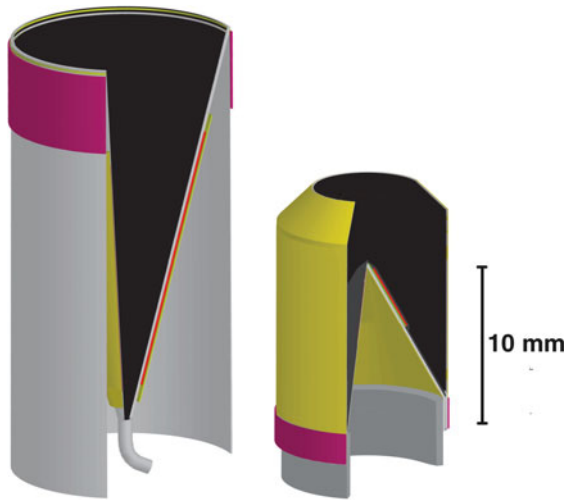


Figure 32.3: The cavities of ACRIM-III (left) and PMO6-V (right). The electrical heaters (red) are wire-wound around the outside of the cone for ACRIM and a flexible printed circuit of Constantan glued to the inverted cone for PMO6V. The temperature sensors (pink) are wire wound around the warm end of the thermal resistor, which is made of silver (ACRIM, light gray as the silver cone) and stainless steel (PMO6V, dark gray); both are soldered to the heat sink.

square-root circuit controlling the heater power in the front cavity. The value is set by the amount of power in the back cavity (REF). The electrical power in the front cavity is measured as voltage drop over the heater and a standard resistor.

First we will discuss the cavities and related effects of the non-equivalence between electrical and radiative heating. Figure 32.3 shows the cavities of ACRIM-III and PMO6-V. The cone angle of ACRIM is 30° and the one of PMO6 60° ; the black paint is in both cases specular. Ideally a ray parallel to the optical axis would undergo six and five reflections for ACRIM and PMO6, respectively, before it leaves the cavity. This would yield a reflectivity of the order of a few 10^{-6} . The measured values for ACRIM and PMO6, however, are of the order of 1.2×10^{-4} and 3.0×10^{-4} , respectively (Willson 1979; Brusa and Fröhlich 1986). The latter is larger because there is no means to reduce the flat part of the tip of the cone of the PMO6 radiometers, whereas ACRIM prevents direct reflections from the bottom with the curved light trap. The thermal resistor of ACRIM is a silver tube soldered to the cone and to the heat sink at the bottom; the one of PMO6 is a stainless steel tube from the inverted cone to the heat sink. A thin copper wire (pink) wound around and glued to the warm end of the thermal resistor serves as the temperature sensor for both radiometers. The electrical heater (red) is wire wound around the cone of ACRIM and covered with aluminized mylar to minimize radiative losses to the outside. The one of PMO6 is a flexible printed circuit made from an etched $5 \mu\text{m}$ Constantan foil forming a 90Ω heater bonded to a $20 \mu\text{m}$ Kapton foil which is directly glued to the front side of the cone and then covered by the black paint. In both radiometers the

heater covers the same area as is illuminated on-axis through the “precision” aperture, an indispensable measure to minimize the non-equivalence. Each radiometer has two receivers in a back-to-back configuration, one for solar measurements and the other as reference of the differential heat-flow meter. The temperature sensor windings of both cavities are elements of a Wheatstone bridge, the output of which regulates the electrical energy dissipated in the primary cavity in such a way that the temperature difference over the thermal resistor is maintained constant. In the case of PMO6V the reference cavity is heated with the same electrical power as used during the reference phase of the operational cavity so that the bridge output can be nulled and does not need to be offset to set the temperature difference.

The effects producing the non-equivalence of these two radiometers are quite different: due to the inverted cone of PMO6 the first reflected radiation does leave the electrically heated part, and produces an extra temperature gradient along the outer shield that is not present in the electrically heated case. In the case of ACRIM some of the electrical heater power may be lost to the outside; in vacuum the effect is probably small due to the radiation shield wrapped around the cone, but it is unknown and uncorrected. In air, however, it is quite large as ground comparisons have shown. For PMO6 the effect is described in [Brusa and Fröhlich \(1986\)](#) and determined from the difference in responsivity in air and vacuum with the argument that the extra losses of the shield in vacuum and thus the non-equivalence are regarded as negligible due to the gold plating of the outside of the shield. This relative correction is rather high with values between 1.5×10^{-3} and 4.0×10^{-3} . The results shown in Table II of [Brusa and Fröhlich \(1986\)](#) indicate, however, that these corrections are well determined, as they reduce the relative standard deviation of the comparison to PMO2 — one of the reference radiometers of the World Radiometric Reference (WRR) — from 1.12×10^{-3} to 0.58×10^{-3} . Moreover, the relative change of the TSI measurement is 2.3×10^{-3} , which corresponds roughly to the average of all the non-equivalence corrections. This turns out to be the most important correction for the PMO6 radiometers with a contribution to the overall 3σ uncertainty of more than one third. For space applications of the PMO6 radiometers this correction is only used to transfer the WRR to space with the results of ground comparison performed in air. In vacuum a corresponding correction is neglected because the losses are only about 3% to 5% of those in air, yielding a small correction of less than 10^{-4} .

Figure 32.4 shows the cavities of DIARAD and TIM. The DIARAD cavity has a flat bottom and uses a diffuse paint. The cone angle of TIM is 30° and the black is not a paint, but an etched nickel phosphorous (NiP) layer deposited inside the silver cone. The measured reflectivities for solar radiation of the cavities are about 2.0×10^{-4} for TIM and 2.5×10^{-4} for DIARAD, which is compatible with the enhancement of such geometries under the assumption of diffuse reflections. In order to avoid direct reflections from the bottom of the cone of TIM a thin and pointed tungsten needle is inserted at the bottom which reflects the radiation back to the cone. The heater of TIM covers the illuminated area of nominally 0.5 cm^2 . For DIARAD the heater covers a circular area of 0.95 cm^2 of which only 0.5 cm^2 or slightly more than 50% is illuminated by the Sun. The radiometers developed at Institut Royal Météorologique de Belgique (IRMB) were the first to arrange both the operational and reference cavities side by side which allows to use both

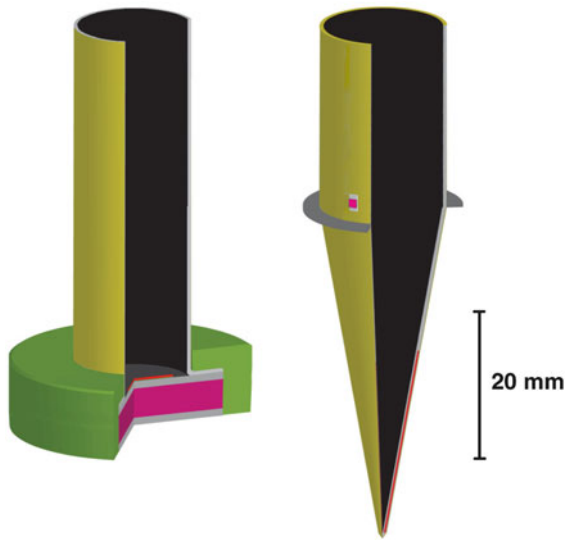


Figure 32.4: The cavities of DIARAD (left) and TIM (right). The electrical heaters (red) are wire-wound around the outside of the cone and encapsulated for TIM, and a flexible printed circuit of Constantan glued to the upper face of the heat flow device (pink) for DIARAD, which is bonded to the heat sink with an indium foil. Three thermistors (pink) soldered to diamond flakes measure the temperature of the cavity for TIM. The thermal resistor to the heat sink is shown schematically as a ring (dark gray) of stainless steel; in reality it is spoked.

alternatively also for solar measurements—hence the name Dual Irradiance Absolute RADiometer. A further important advantage of this arrangement is that it provides a very similar thermal environment to both receivers, which substantially reduces the sensitivity to changes of temperature and related gradients by, e.g., eclipses during a low Earth orbit, producing thermal waves from the front to the back. In TIM this arrangement is extended to two pairs which allows now simultaneous measurements and comparison of each of the two detector pairs.

The effects of the non-equivalence for DIARAD and TIM are quite different. For DIARAD the non-equivalence is due to the difference in the area which is irradiated and electrically heated and due to radiation reflected from the bottom to the sidewall, a similar effect as for the PMO6 cavities. With results from mapping the sensitivity over the bottom of the cavity and along the sidewall with a laser beam, a corresponding correction—called *efficiency* (Crommelynck 1989)—is estimated. In vacuum, the relative correction amounts to 1.3×10^{-4} for DIARAD on VIRGO (Crommelynck and Dewitte 2005).

The accurate knowledge of the size of the “precision” aperture is obviously very important—it defines the area in which the solar radiation is collected. Figure 32.1 illustrates the importance very nicely as the differences in the early measurements were mainly due to the uncertainty of the aperture area. Both, the manufacturing of precise and round apertures with short or zero land (cylindrical part of the

aperture) and the measurement techniques, have been substantially improved during recent years and allow now for relative uncertainties as low as $(5 \text{ to } 10) \times 10^{-5}$ (Johnson et al 2003; Litorja et al 2007) for apertures with diameters of 5 mm to 8 mm. The apertures of ACRIM, PMO6V and DIARAD are made of stainless steel and turned or milled to shape. The one of DIARAD is covered with a thin layer of evaporated nickel, the surfaces of the others are as manufactured. The TIM aperture is made from nickel-covered aluminium which is diamond-turned to shape. In the classical radiometers the “precision” apertures are placed directly in front of the cavities, and a further aperture at about 100 mm to 140 mm from the “precision” aperture limits the field of view to approximately 5° full angle with an angle of 1° between the opening of the apertures, called slope. This is compatible with the view-limiting geometry of pyrhelimeters used on ground for solar radiometry and allows direct comparison with, e.g., the World Radiometric Reference (see, e.g., Fröhlich 1991), maintained at PMOD/WRC in Davos. TIM has the aperture geometry inverted with the “precision” aperture (8 mm) at the front of the instrument and the viewing angle is limited by the diameter of the cavity entrance (16 mm at 104 mm behind the “precision” aperture). This obviously needs a large cavity with a rather long time constant, which is, however, no problem for TIM as it is not operated in a quasi-steady-state mode as the classical radiometers.

From the beginning of solar radiometry in the sixties one was concerned about possible heating of the “precision” aperture directly in front of the cavity which would emit additional IR radiation into the cavity. This IR radiation is proportional to the solar irradiance and hence results in an increase of responsivity. In the early seventies tests with electrical heaters were performed (see, e.g., Geist 1972), but no conclusive results were obtained, mainly because the emphasis was more on how much the overall temperature of the aperture increased than on the detailed temperature distribution especially at the edge of the aperture. This edge has a short enough thermal time constant for the temperature to rise and fall during the shuttered operation and thus to contribute to the signal in the cavity, whereas an overall temperature increase of the aperture does not influence the measurement. This effect is very difficult to determine experimentally. The problem came back with the detection of the early increase of the responsivity of the PMO6 radiometer in VIRGO (Fröhlich et al 1997), which can partly be explained by a steadily increasing aperture heating due to, e.g., a blackening of the aperture due to the strong solar UV radiation from, e.g., $\text{Ly}\alpha$ during the early exposure of the radiometer. Inspection of the apertures of the PMO6 type radiometers of SOVA-2 which were in space for more than one year during the *EURECA* mission and then retrieved showed indeed a blackening of the apertures. More recent investigations show, however, that the relative aperture heating is with $\approx 0.03\%$ rather small (Fröhlich 2010). An early increase of similar magnitude is also observed in the HF, ACRIMs and ERBE radiometers (Fröhlich 2003, 2006); as these radiometers use different materials for the apertures the effect may more likely be explained by a change of the absorptivity of the specular paint in these cavities. Due to the nickel plating of the DIARAD aperture and due to the use of a diffuse paint no early increase effect is observed.

The difference in absolute values between the classical radiometers and TIM is most likely related to the arrangement of the apertures and more specifically to

increased scattered light from the view-limiting aperture. To investigate this difference experimentally the TSI Radiometer Facility (TRF) was developed at LASP and allows an overall assessment of these effects by comparing the measurements directly with a cryogenic reference radiometer (Kopp et al 2007). The work at the TRF is not complete, but already appears to require the changes discussed by Kopp and Lean (2011). The results for a spare PMO6V radiometer of VIRGO (in Kopp and Lean 2011, called VIRGO2) indicate a scattered light contribution of only 0.154%. Even by adding an estimated aperture heating of 0.03% (Fröhlich 2010) the effect is too small to explain the difference. As the PMO6V radiometers are referenced to the World Radiometric Reference (WRR) the remaining difference is most likely one of scales of SI and WRR (see, e.g., Finsterle et al 2008). Moreover, there are still no results available for the DIARAD radiometers. On the other hand, the recent TRF tests with an ACRIM III spare confirm the difference and the new version 11/05 of the ACRIM data base yield values close to those of TIM as shown in Figure 32.1. Although no final results for VIRGO radiometry are available, the PMOD composite may be adjusted as an intermediate solution to the TIM value during the 2008/9 minimum by multiplying it by 0.996894. The conclusion is that the TSI value during the recent minimum is closer to 1361 than to 1365 W m^{-2} .

Diffraction is another effect which needs to be included in the corrections. This correction depends on the relative arrangement of the two apertures. If the larger aperture is in front of the radiometer, its diffraction adds radiation through the “precision” aperture due to Babinet’s theorem. In the other case, the “precision” aperture in front diffracts radiation out of the view-limiting aperture, reducing the received radiation. In other words, the amount diffracted out is greater than the amount diffracted in. Thus, the aperture arrangement of the classical radiometers leads to a relative increase of the measured radiation by $(0.2 \text{ to } 1.3) \times 10^{-3}$ depending on the size of their apertures and the distance between them, and reduces it for TIM by 4.2×10^{-4} (Brusa and Fröhlich 1986; Kopp et al 2005a; Shirley 1998). These corrections are calculated from theory which is based on exactly co-aligned and circular apertures; nevertheless, their relative uncertainties seem to be at the level of a few percent.

Another important aspect of solar radiometry is the influence of the immediate thermal environment seen by the detector. Most important is the difference in IR radiation received by the cavity during the shutter open and closed phases, respectively. Temperature sensors in the front part of the radiometers and on the shutter, together with thermal models, are used to estimate and correct these effects. An obvious test for these estimates is measurement of the radiation from deep space. Other effects for the characterization like stray light and lead¹ heating have been described in some detail (Willson 1979; Brusa and Fröhlich 1986; Crommelynck and Dewitte 2005; Kopp and Lawrence 2005) and will not be discussed further. Problems related to the electrical power measurements and their uncertainties are also not discussed here, but details from the VIRGO experiment as an example can be found in Fröhlich et al (1995, 1997).

¹i.e., electrical connections

Operation of solar radiometers

Classical radiometers are operated in a quasi-stationary mode with shutter cycles of 60 s to 90 s. At the end of each phase the electrical power is read and the irradiance S evaluated according to

$$S = \frac{C}{A}(P_{\text{closed}} - P_{\text{open}}) \quad , \quad (32.1)$$

with A the area of the “precision” aperture and C the total correction factor as determined by characterization. P_{closed} and P_{open} are the closed and open electrical power readings. This operation relies on a rather short time constant which is improved with the overall gain of the servo loop which is typically between three and five. So, an open-loop or natural $1/e$ time constant of about 20 s is reduced to 4 s to 7 s. Normally, there is not only one measurement before the end of a phase, but a few, so that the servo-loop characteristics can also be checked in flight. In contrast to this classical active-mode operation TIM uses phase-sensitive detection at the fundamental shutter period. This avoids many problems with effects at higher frequencies. For the behaviour of the non-equivalence in the classical case one needs to take into account all contributions from frequencies of up to at least ten times the shutter frequency because a full square wave has to be reconstructed. The TIM radiometer is operated in the same way as the classical radiometers, that is, the electrical power is always adjusted so that the temperature difference — or the heat flux — remains constant. The electrical power is derived from a constant voltage source with pulse-width modulation. The evaluation of the phase-sensitive signal is somewhat more complicated because most terms are complex phasor components representing the amplitude and phase of sinusoidal variations (indicated as bold-type symbols). With A for the aperture area and α for the absorptivity of the cavity, the irradiance S is evaluated from the time series of the fraction \mathbf{D} of the electrical power P_0 as

$$S = \frac{P_0}{\alpha A} \operatorname{Re} \left[-\frac{\mathbf{Z}_{\text{el}}}{\mathbf{Z}_{\text{rad}}} \frac{1}{\mathbf{T}} \left(\mathbf{D} + \frac{\mathbf{D} - \mathbf{F}}{\mathbf{G}} \right) \right] \quad , \quad (32.2)$$

which corrects also for the complex servo system gain \mathbf{G} , the shutter timing \mathbf{T} , and the equivalence as ratio of the corresponding impedances $\mathbf{Z}_{\text{el}}/\mathbf{Z}_{\text{rad}}$ and the applied feed-forward values \mathbf{F} at the shutter frequency. This latter effect accelerates the control system with the information of the last shutter-open values fed forward. The time series of the instantaneous fraction of power fed to the cavity \mathbf{D} is generated from a pulse-width modulator controlled by a digital signal processor maintaining the thermal balance of the cavity. This signal is sampled at 100 Hz and transmitted to ground as numbers from 0 to 64 000, representing the fraction $q = D/64\,000$ of P_0 . The advantage of the transmission of \mathbf{D} is obviously that one can also analyse other frequency terms for diagnostics by choosing a different \mathbf{T} . The final S is convoluted with a Gaussian filter of about 400 s width. This means that fluctuations due to, e.g., p modes cannot be resolved, but for the objective of TSI for Sun-Earth connections this seems justified. Due to the fact that the result is a true integral the aliases due to such higher-frequency variations are suppressed anyway.

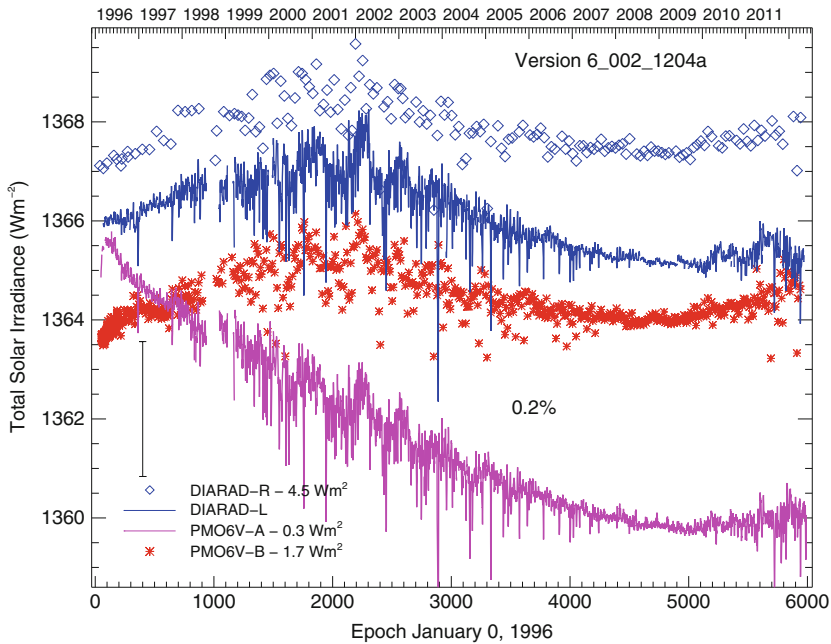


Figure 32.5: Level-1 data of the two radiometers on VIRGO: DIARAD-L and R and PMO6V-A and B. Note the difference in the amount of degradation of PMO6V-A relative to DIARAD-L and the early increase of the PMO6V-A and B (Lower abscissa in days).

The value of TSI as determined from the above algorithms includes all known instrumental effects. It has to be normalized to 1 ua, the mean Sun-Earth distance, by multiplying the measured value by $(r_E/\text{ua})^2$, the actual value of the Sun-instrument distance being r_E . The relative correction varies between $\pm 3\%$ and can be done to a relative uncertainty of at least 1.0×10^{-7} from the ephemeris of the spacecraft. A further correction is needed for the Doppler effect due to the radial velocity between the source and the radiometer. The correction is discussed in Chapter 2 (Wilhelm and Fröhlich 2013) and is proportional to $(1 - 2v_r/c_0)$ with v_r being positive away from the Sun. For a low-orbit satellite this correction can amount to up to $\pm 6 \times 10^{-5}$ with radial velocities of up to $\pm 9 \text{ km s}^{-1}$.

Long-term behaviour of solar radiometers in space

From Figure 32.5 it is obvious that the long-term behaviours of the four VIRGO radiometers differ substantially from each other, and important corrections are needed to deduce a reliable TSI from these data. Already at this stage of the evaluation the different long-term behaviour of the operational PMO6V and DIARAD is very obvious. Also prominent is the early increase of the PMO6V radiometers during the first weeks of exposure. From the comparison of a back-up instrument of the same type with much less exposure to solar radiation, changes due to ex-

posure to the Sun can be determined. But these data are sparse and we need a reliable way to interpolate between the reference measurements in order to enable continuous correction of the operational radiometer. One may use fitting of polynomials of higher degrees (Willson and Hudson 1991; Willson and Helizon 2005) or one can use some other methods, e.g., running means (Dewitte et al 2004a). A much better way is to use a model which also helps to understand the physical mechanisms. Such a model is based on a hyperbolic function (e.g., Fröhlich and Anklin 2000; Fröhlich and Finsterle 2001; Fröhlich 2006) which is the solution of the differential equation describing the “siliconizing” of a quartz window exposed to UV radiation, that is, a change of the optical properties due to the formation of silicon at the surface with a subsequent decrease of the response of the underlying quartz to radiation exposure. The time-dependent sensitivity change $\Delta S(t)$ with t_{exp} for the exposure time can be described as

$$\Delta S(t) = a \left[\left(1 + \frac{1}{b \tau_C} \int_0^{t_{\text{exp}}} (\lambda m(t) + 1) dt \right)^{-b} - 1 \right] \quad (32.3)$$

with a, λ, b and $1/(b \tau_C)$ as adjustable parameters. The parameter b has been included in τ_C , which then corresponds to a $1/e$ time constant. This transforms the hyperbolic function to an exponential for large b , reducing the number of parameters:

$$\Delta S(t) = a \left[\exp \left(-\frac{1}{\tau_C} \int_0^{t_{\text{exp}}} (\lambda m(t) + 1) dt \right) - 1 \right]. \quad (32.4)$$

Although for $b < 20$ the differences are substantial a fit with Eq. 32.4 shows good overall agreement. So the hyperbolic function can be replaced with the exponential one in all cases, which simplifies the analysis. The integral corresponds to the dose received during the exposure time, and for $m(t)$ the Mg II index is used as surrogate for the UV radiation, normalized to -0.5 to 0.5 . The fitted parameter λ provides the information about the wavelength responsible for the effect as it is proportional to the cycle variability of the corresponding wavelength, and 2λ corresponds to the cycle amplitude of that radiation. Thus, for, e.g., Ly α with a solar cycle variation of $(0.06$ to $0.10) \text{ mW m}^{-2}$ (Rottman et al 2004), $\lambda = (1/2)(0.1/0.06) = 0.83$. This analysis not only explains the dose dependence of the changes, but also provides information about the physical mechanisms behind it.

In the case of VIRGO this analysis works only for the PMO6V radiometers, mainly because the changes of DIARAD are a mixture of exposure-dependent and also non-exposure-dependent changes. For an illustration of the method, the behaviour of ACRIM-I is shown in Figure 32.6 and the hyperbolic function of the degradation explains the behaviour quite well. The correction of the early increase is not shown here, for details of this correction see Figure 2 of Fröhlich (2006). It shows also how important the dose is, and that neither the exposure time alone nor a simple polynomial fit is sufficient — especially if the activity level is changing during the period analysed.

For the PMO6V on VIRGO this analysis is complicated by the fact that also the back-up instrument was exposed more than normally due to the change in

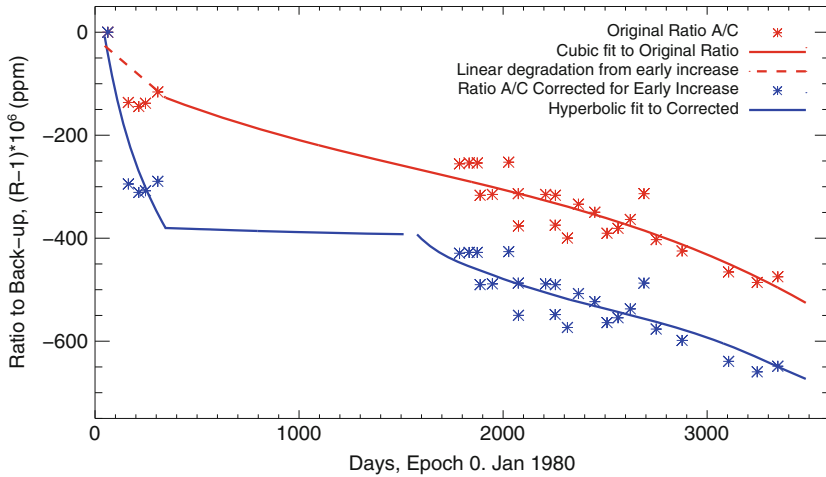


Figure 32.6: The original ratios of sensor A to sensor C (red symbols) of the ACRIM-I experiment on *SMM* are from Willson and Hudson (1991). The cubic fit corresponds to the correction originally applied and the dashed line includes the linear fit found by fitting the early increase (not shown). The blue symbols are corrected for the early increase and then fitted with a hyperbolic function. Note the dose-dependent change over the period of the spin mode (roughly after day 2700 on the time axis) and after the solar minimum of 1986 (after day 2100). Adapted from Figure 3 of Fröhlich (2006).

operations (Fröhlich et al 1997). Thus, it shows a significant early increase which has to be corrected before the back-up can be used for the determination of the exposure-dependent changes of PMO6V-A. The principles of these dose-dependent corrections are described in Fröhlich (2003), however, for version 5. Since then the exposure-dependent changes of PMO6V have been revised for version 6 as well as the corresponding non-exposure-dependent changes of DIARAD. This has improved the internal consistency of the corrections substantially. The most recent VIRGO results (version 6.2, updated to end of March 2012) are shown in Figure 32.1; they are the basis for the PMOD composite. Also included in Figure 32.1 is the DIARAD time series which is determined from the DIARAD-L and R alone (updated from Dewitte et al 2004a). Their analysis assumes arbitrarily that there is no change over the *SOHO* “vacations” (i.e., the loss of Sun-pointing attitude from June to September 1998) which is not confirmed by comparison with, e.g., ACRIM-II and ERBE. Besides this obvious misinterpretation, the overall behaviour shows a weaker decrease over solar cycle 23 than any other time series during this period. This is due to the neglect of the non-exposure-dependent increase of sensitivity which cannot be assessed by analysing the operational and the back-up radiometer alone. It can only be detected by comparison with an independent radiometer, e.g., PMO6V. Albeit this effect was not anticipated before launch, the reason for having two different radiometers within VIRGO was: “Although the designs of both radiometers are based on the same principle, the physical realization is different” (from Fröhlich et al 1995). The residuals of the comparison

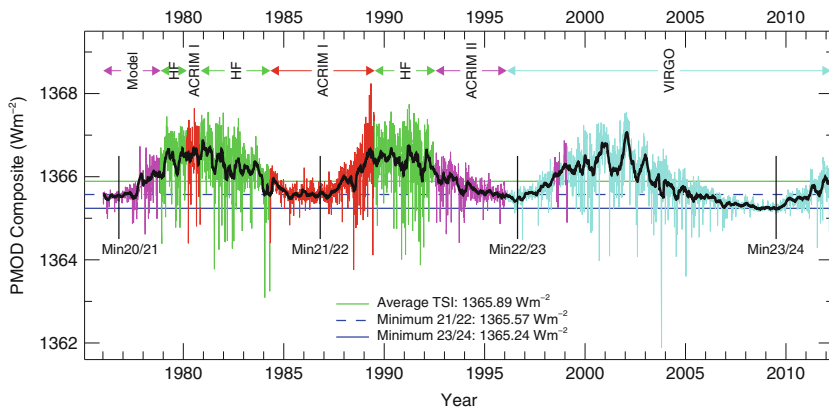


Figure 32.7: Shown is the PMOD composite (version 41_62_1204), updated to end of March 2012 with an extension back 1975 based on a proxy model (see e.g. Fröhlich 2011). The minima values as one-year averages amount to (1365.53, 1365.57, 1365.47, 1365.23) W m^{-2} with an average of 1365.46 W m^{-2} and the amplitudes of three cycles are (0.9493, 0.9165, 0.9124) W m^{-2} . In contrast to cycles 21 and 22 there is a substantial trend over cycle 23 with a difference between the two adjacent minima amounting to a change of 26% relative to the amplitude of this cycle (see, e.g., Fröhlich 2009, 2012), which is a very interesting and important result.

of DIARAD and PMO6V, both corrected for exposure-dependent changes (level-1.8), can now be fitted to an exponential function which describes the long-term sensitivity change. Comparisons with ACRIM-II/III or ERBE instead of PMO6V yield essentially the same results, indicating that it is indeed a sensitivity change of DIARAD. The need for such a correction of DIARAD is also confirmed by the measurements with a similar DIARAD-type radiometer within the SOVIM experiment (Mekaoui et al 2010) on the International Space Station (*ISS*), which lie very close to VIRGO TSI. A similar effect is also found for the HF as shown in Fröhlich (2006). So, these two radiometers show an increase of sensitivity which is independent of exposure to radiation and fortunately no such effect is present in ACRIM, ERBE and PMO6 radiometers. Thus, the DIARAD/VIRGO data as published by Dewitte et al (2004a) and Dewitte et al (2004b) are confusing and are not correctly representing the irradiance from the Sun, instead the VIRGO results should be used (see also Fröhlich 2012).

Results and discussion of solar radiometry

With the VIRGO TSI data for solar cycle 23 and the data from HF, ACRIM-I and -II for the period before 1996 we can construct a composite TSI as described in Fröhlich (2006), and in Figure 32.7 the so-called PMOD composite is shown as an example. There are two other composites from the ACRIM (Willson and Mordvinov 2003) and IRMB (Dewitte et al 2004b) teams. The differences between these and the PMOD composite have been discussed extensively in Fröhlich (2006, 2009) and

Lockwood and Fröhlich (2007, 2008), where also detailed information about the reasons for the differences can be found. Figure 32.7 shows very interesting results of solar variability during the last three solar cycles. Most importantly, the most recent minimum is lower than the previous ones, and the length of this last solar cycle is also much longer than the previous ones.

The results show that overlapping measurements from different platforms enable to construct a reliable TSI record, demonstrating that the relative precision of the individual radiometers is much higher than their uncertainty. The result also shows that only a detailed understanding of the degradation helps to correct the data over longer periods than the 11-year solar cycle. Comparison with simultaneous TSI measurements from ACRIM-II and III and TIM/*SORCE* indicate that VIRGO may overestimate this trend (Fröhlich 2009), but a relative change of at least 18 % (instead of the 26 % stated in Figure 32.7) can be confirmed. With a long-term stability of $\pm 3.5 \times 10^{-5}$ per decade (Fröhlich 2004) and $\pm 5.0 \times 10^{-5}$ per decade (Fröhlich 2009) the presently observed low value of TSI is significant, but different from what is observed in *spectral* irradiance (see Figure 2.3 of Chapter 2) which shows relative changes of less than 5% between minima. This means that there are different physical mechanisms responsible for the trend in TSI and the cycle variation of TSI and SSI. The former could be due to a long-term change in the photospheric temperature which only marginally influences UV radiation of the Sun (Tapping et al 2007; Fröhlich 2009). Another explanation was recently put forward by Foukal et al (2011) based on the effect of the increasing contrast of the network and faculae with decreasing magnetic flux density. This effect is confirmed by Schnerr and Spruit (2011) who evaluated high-resolution polarimetric observations with the 1 m Swedish Solar Telescope (SST) and *Hinode* and could well be the explanation of the difference between TSI, formed in the photosphere, and UV radiation formed in the chromosphere.

In conclusion, solar radiometry from space has proven its ability to produce reliable records of TSI over more than 30 years. This result is not only important by itself, but helps to improve our understanding of the behaviour of the Sun and its influence on the climate of Earth.

Acknowledgements

The author would like to thank Greg Kopp, LASP at University of Colorado, Steven Dewitte and Andre Chevalier, Institut Royale Météorologique de Belgique, Richard Willson, Columbus University, for many helpful discussions about their radiometers. And last but not least all these results would not have possible without the continuing support of the Swiss National Science Foundation, and the *SOHO* and VIRGO Teams, which is gratefully acknowledged. *SOHO* is a cooperative mission of ESA and NASA.

References

- Abbot C (1952) Periodicities in the solar-constant measures. *Smithsonian MiscColl* 117(10):1–31

- Aldrich L, Hoover W (1954) Annals of the Astrophysical Observatory of the Smithsonian Institution, vol 7, Smithsonian Institution, Washington, DC, U.S.A., chap 7: Statistical Studies of the Solar-Constant Record, pp 165–168
- Brusa RW, Fröhlich C (1986) Absolute radiometers (PMO6) and their experimental characterization. *Appl Opt* 25:4173–4180
- Crommelynck D (1989) Factors limiting the accuracy of absolute radiometry. In: *New Developments and Applications in Optical Radiometry* (ed N Fox) Inst Phys Conf Ser 92, London, pp 19–24
- Crommelynck D, Dewitte S (2005) The DIARAD type instruments: Principles and error estimates, presented at the “Total Solar Irradiance Workshop” at NIST, Gaithersberg, Md, USA, 18–20 July 2005
- Crommelynck DA, Brusa RW, Domingo V (1987) Results of the solar constant experiment onboard Spacelab 1. *Sol Phys* 107:1–9
- Dewitte S, Crommelynck D, Joukoff A (2004a) Total solar irradiance observations from DIARAD/VIRGO. *J Geophys Res* 109:A02102
- Dewitte S, Crommelynck D, Mekaoui S, Joukoff A (2004b) Measurement and uncertainty of the long-term total solar irradiance trend. *Sol Phys* 224:209–216
- Drummond AJ, Hickey JR, Scholes WJ (1968) New value for the solar constant of radiation. *Nature* 218:259–261
- Finsterle W, Blattner P, Moebus S (plus four authors) (2008) Third comparison of the World Radiometric Reference and the SI radiometric scale. *Metrologia* 45:377–381
- Foukal P, Ortiz A, Schnerr R (2011) Dimming of the 17th Century Sun. *Astrophys Journal Lett* 733:L38
- Fröhlich C (1977) Contemporary measures of the solar constant. In: *The Solar Output and its Variation* (ed. OR White), Colorado Associated Univ. Press, Boulder, pp 93–109
- Fröhlich C (1991) History of solar radiometry and the World Radiometric Reference. *Metrologia* 28:111–115
- Fröhlich C (2003) Long-term behaviour of space radiometers. *Metrologia* 40:60–65
- Fröhlich C (2004) Solar irradiance variability. In: *Geophysical Monograph 141: Solar Variability and its Effect on Climate*, American Geophysical Union, Washington DC, USA, chap 2: Solar Energy Flux Variations, pp 97–110
- Fröhlich C (2006) Solar irradiance variability since 1978: Revision of the PMOD composite during solar cycle 21. *Space Sci Rev* 125:53–65
- Fröhlich C (2009) Total solar irradiance variability: What have we learned about its variability from the record of the last three solar cycles? In: *Climate and Weather of the Sun-Earth System(CAWSES): Selected Papers from the 2007 Kyoto Symposium, October, 23–27 2007*, (eds T Tsuda, R Fujii, K Shibata, M Geller) Terra Publishing, Setagaya-ku, Tokyo, Japan, 217–230
- Fröhlich C (2010) Possible Influence of Aperture Heating on VIRGO Radiometry on *SOHO*. AGU Fall Meeting Abstracts B874
- Fröhlich C (2011) A four-component proxy model for total solar irradiance calibrated during solar cycles 21–23. *Contrib Astron Obs Skalnat Pleso* 41:113–132
- Fröhlich C (2012) Total solar irradiance observations. *Surveys in Geophysics* 33 (3–4):453–473

- Fröhlich C, Anklin M (2000) Uncertainty of total solar irradiance: An assessment of the last 20 years of space radiometry. *Metrologia* 37:387–391
- Fröhlich C, Finsterle W (2001) VIRGO radiometry and total solar irradiance 1996–2000 revised. *ASP Conf Ser* 203:105–110
- Fröhlich C, Romero J, Roth H (plus 21 authors) (1995) VIRGO: Experiment for helioseismology and solar irradiance monitoring. *Sol Phys* 162:101–128
- Fröhlich C, Crommelynck D, Wehrli C (plus seven authors) (1997) In-flight performances of VIRGO solar irradiance instruments on *SOHO*. *Sol Phys* 175:267–286
- Geist J (1972) Fundamental principles of absolute radiometry and the philosophy of this NBS program (1968–1971). In: NBS Technical Note 594-1, U.S. Department of Commerce, National Bureau of Standards, Gaithersburg, Md, USA
- Johnson BC, Litorja M, Butler JJ (2003) Preliminary results of aperture-area comparison for exo-atmospheric solar irradiance. *Proc SPIE* 5151:454–462
- Kopp G, Lawrence G (2005) The Total Irradiance Monitor (TIM): Instrument design. *Sol Phys* 230:91–109
- Kopp G, Lean JL (2011) A new, lower value of total solar irradiance: Evidence and climate significance. *Geophys Res Lett* 38:L01706
- Kopp G, Heuerman K, Lawrence G (2005a) The Total Irradiance Monitor (TIM): Instrument calibration. *Sol Phys* 230:111–127
- Kopp G, Lawrence G, Rottman G (2005b) The Total Irradiance Monitor (TIM): Science results. *Sol Phys* 230:129–139
- Kopp G, Heuerman K, Harber D, Drake G (2007) The TSI Radiometer Facility: absolute calibrations for total solar irradiance instruments. In: Society of Photo-Optical Instrumentation Engineers (SPIE) Conference Series 6677, DOI 10.1117/12.734553
- Litorja M, Johnson BC, Fowler J (2007) Area measurements of apertures for exo-atmospheric solar irradiance for JPL. *Proc SPIE* 6677:667–708
- Lockwood M, Fröhlich C (2007) Recent oppositely directed trends in solar climate forcing and the global mean surface air temperature. *Proc R Soc A* 463:2447–2460
- Lockwood M, Fröhlich C (2008) Recent oppositely-directed trends in solar climate forcings and the global mean surface air temperature: II. different reconstructions of the total solar irradiance variation and dependence on response timescale. *Proc R Soc A* 464:1367–1385
- Mekaoui S, Dewitte S, Conscience C, Chevalier A (2010) Total solar irradiance absolute level from DIARAD/SOVIM on the International Space Station. *Advances in Space Research* 45:1393–1406
- Plamondon J (1969) The Mariner Mars 1969 temperature control flux monitor. *JPL Space Prog Summary* 37–59, Vol.III(37–59):162–168
- Rottman G, Floyd L, Viereck R (2004) Measurement of the solar ultraviolet irradiance. *Geophysical Monograph* 141:111–126
- Schnerr RS, Spruit HC (2011) The Total Solar Irradiance and Small Scale Magnetic Fields. *ASP Conf Ser*, vol 437:167–175
- Shirley EL (1998) Revised formulas for diffraction effects with point and extended sources. *Appl Opt* 37:6581–6590

-
- Tapping KF, Boteler D, Charbonneau P (plus three authors) (2007) Solar Magnetic Activity and Total Irradiance Since the Maunder Minimum. *Solar Phys* 246:309–326
- Wilhelm K, Fröhlich C (2013) Photons—from source to detector. ISSI SR-009:21–53
- Willson RC (1972) Experimental comparisons of the International Pyrheliometric Scale with the absolute radiation scale. *Nature* 239:208–209
- Willson RC (1979) Active cavity radiometer type iv. *Appl Opt* 18:179–188
- Willson RC (2001) The ACRIMSAT/ACRIM III Experiment: Extending the precision, long-term total solar irradiance climate database. *The Earth Observer* 13:14–17
- Willson RC, Hudson HS (1991) The Sun’s luminosity over a complete solar cycle. *Nature* 351:42–44
- Willson R, Helizon R (2005) Active cavity radiometer irradiance monitors: S.I. measurements uncertainties, presented at the “Total Solar Irradiance Workshop” at NIST, Gaithersberg, Md, USA, 18–20 July 2005
- Willson RC, Mordvinov AV (2003) Secular total solar irradiance trend during solar cycles 21–23. *Geophys Res Lett* 30:1199